Radio emission from the Composite supernova Remnant G326.3-1.8 (MSH 15-56)

Dickel, H.R.; Milne, A.B.; Strom, R.G.

Link to publication

RADIO EMISSION FROM THE COMPOSITE SUPERNOVA REMNANT G326.3−1.8 (MSH 15−56)

JOHN R. DICKEL[1]
Astronomy Department, University of Illinois at Urbana-Champaign, Urbana, IL 61801; johnd@astro.uiuc.edu

D. K. MILNE
Australia Telescope National Facility, Epping NSW 1710, Australia; dmilne@atnf.csiro.au

AND

RICHARD G. STROM[2]
Netherlands Foundation for Research in Astronomy (ASTRON), 7990AA Dwingeloo, Netherlands; strom@nfra.nl
Received 2000 May 26; accepted 2000 June 16

ABSTRACT

High-resolution radio observations of the composite supernova remnant (SNR) G326.3−1.8, or MSH 15−56, with the Australia Telescope Compact Array show details of both the shell and the bright plerion, which is offset about one-third of the distance from the center of the SNR to the shell. The shell appears to be composed of thin filaments, typical of older shell SNRs. The central part of the elongated plerion is composed of a bundle of parallel ridges that bulge out at the ends and form a distinct ring structure on the northwestern end. The magnetic field, with a strength of order 45 μG, is directed along the axis of the ridges but circles around the northwestern ring. This plerion is large and bright in the radio but is not detected in X-ray or optical wavelengths. There is, however, a faint hard X-ray feature closer to the shell outside the plerion. Perhaps, if the supernova explosion left a rapidly moving magnetar with large energy input but initially rapid decay of both relativistic particles and magnetic field, the observed differences with wavelength could be explained.

Subject headings: ISM: individual (G326.3−1.8) — polarization — pulsars: general — radiation mechanisms: nonthermal — radio continuum: ISM — supernova remnants

1. INTRODUCTION

The supernova remnant (SNR) G326.3−1.8, or MSH 15−56 (Mills, Slee, & Hill 1961), is the prototype of the class of composite SNRs containing a shell with a relatively steep radio spectrum and an interior flat-spectrum plerion component (Weiler & Sramek 1988). In some composite SNRs a pulsar is observed in the plerion, e.g., 0540−693 in the Large Magellanic Cloud (Seward, Harnden, & Helfand 1984; Manchester, Stavely-Smith, & Kesteven 1993), but in a number of others, including G326.3−1.8, no pulsar has been detected. In all cases, however, a pulsar is presumed to be present to inject high-energy particles into the plerion component. The lack of detection is attributed to a misalignment of the pulsar's axis so that its beam does not cross the Earth. Alternatively, the pulsar may be very old and faint, so more sensitive surveys are needed to detect it or the pulsed emission may have ceased altogether.

The shell, on the other hand, is produced by the interaction of supersonic ejecta from the explosion and swept-up material from the surroundings. Strong shocks heat the gas to produce X-rays and accelerate particles to relativistic speeds, which, together with magnetic fields amplified in the interaction zone, produce synchrotron radiation. Subsequent cooling and compression of the shocked gas can locally increase the synchrotron emission and also produce optical recombination line emission.

There is a great range of relative sizes and brightnesses of the plerion and shell components in composite remnants. The large size and high brightness of the plerion in G326.3−1.8 place it near the extreme in each category. It fills about 0.04 of the area and has about 0.20 of the integrated flux density of the entire remnant. By contrast, the well-known SNR W44 represents the other end of the range for comparison: its plerion covers only about 0.0025 of the area and has a flux density of 0.001 that of the entire SNR (Giacani et al. 1997; Frail et al. 1996).

To understand the relation between the different components and how they might evolve, we need detailed studies of both the shell and the plerion in several composite SNRs covering the full range of parameters from G326.3−1.8 to W44. G326.3−1.8 has been investigated at a number of wavelengths. The highest resolution radio images to date are from the Molonglo Observatory Synthesis Telescope (MOST) at 0.843 GHz (Kesteven & Caswell 1987; Milne et al. 1989; Whiteoak & Green 1996) and from the Fleurs Synthesis Telescope at 1.414 GHz (Milne et al. 1989); both had half-power beamwidths of about 45″. These show the faint, rather incomplete shell but were unable to resolve fine-scale features within the plerion. The shell is slightly noncircular with a diameter between about 40′ and 35′. The plerion is displaced about 7′ to the southeast from the center of the SNR; its outline is irregular but is contained within an ellipse having axes of 10′ × 5′. The long axis is aligned approximately southeast-northwest. The best polarimetry available, by Milne et al. (1989), has a resolution of 3′ at 8.4 GHz. The plerion is strongly polarized with the magnetic field aligned approximately along its major axis.

The X-ray emission also shows shell structure in some locations (Kassim, Hertz, & Weiler 1993). Extended features in both hard and soft X-rays appear within the interior, although they show no correspondence to the radio plerion nor to other features seen in the radio or optical (Plucinsky 1998). Optical filaments are present around parts of the shell and on the face of the SNR (van den Bergh 1979; Zealey, Elliott, & Malin 1979) but, again, show little rela-

---

TABLE 1

OBSERVING PARAMETERS

FREQUENCY (GHz)	HPBW (arcsec)	RMS NOISE (mJy beam^{-1})		FLUX DENSITY OF PKS B1934−638 (Jy)
		Total Intensity	Polarized Intensity	
1.34	8.5 × 6.4[a]	1.70	0.13	15.01
4.80	3.8 × 3.8	1.30	0.05	5.83
8.64	3.2 × 3.2	0.80	0.10	2.84

[a] Long axis at position angle 11°.

tion to any radio features. The filaments show a high ratio of [S II]/Hα, which is typical of shocked material in radiative equilibrium (Dennefeld 1980).

Although the plerion is unseen in the other wavelength ranges, it is clearly an important part of the SNR. Its radio synchrotron emission is strong, implying a large content of low-energy relativistic electrons but apparently a rapid loss of high-energy ones. Determination of structure within the plerion may help establish the relation to any pulsar. Other characteristics can give indications of its relation to other parts of the SNR and its evolution within it. In addition, it is important to do a sensitive search for any radio counterparts to the various X-ray features seen in the remnant.

We adopt the kinematic distance determined from an Hα radial velocity measurement by Rosado et al. (1996) of 4.1 kpc. This value is compatible with a visual extinction measurement of greater than 5.1 mag by Dennefeld (1980) and a 21 cm absorption measurement of greater than 1.5 kpc by Caswell et al. (1975). At this distance, the outer edge of the shell of G326.3−1.8 has dimensions of 48 × 42 pc, and the extent of the irregular boundary of the plerion is about 12 × 6 pc.

To investigate the radio structure and polarization in detail we have observed G326.3−1.8 with the Australia Telescope Compact Array (ATCA). Polarimetric images of the plerion and its near environs have been obtained at 4.8 and 8.64 GHz, while the entire SNR has been imaged at 1.34 GHz. These observations reveal the detailed structure of the plerion and its polarization for the first time. The equipment and observations are described in § 2, the results

are presented in § 3, the interpretation is discussed in § 4, and a summary is in § 5.

2. EQUIPMENT AND OBSERVATIONS

The ATCA (Frater, Brooks, & Whiteoak 1992) can record both 1.34 and 2.4 GHz simultaneously or both 4.8 and 8.64 GHz simultaneously. Both pairs of frequencies were observed, but the data at 2.4 GHz were seriously degraded by interference and not used in the analysis. Each set of observations was done with four separate antenna configurations, giving a total of 54 independent baselines covering a range of spacings from 31 to 6000 m. The observing parameters are given in Table 1. The beams at the two higher frequencies were nearly round and so were restored with circular half-power beamwidths, but the more elliptical beam at 1.34 GHz, with an HPBW of 8".5 × 6".4 at a position angle of 11°, was left with its original elliptical dimensions.

The large angular size and low surface brightness of G326.3−1.8 required long-integration, full-synthesis mosaic observations. At 1.34 GHz, the entire SNR was covered by a 16-point mosaic pattern with pointings spaced by 11′. At 4.8 and 8.64 GHz it was decided to concentrate only on the bright plerion component. This region was covered by a 25-point mosaic with spacings of 2′.5, which was just under the half-width of the primary beam pattern at 8.64 GHz.

The observing bandwidth was 128 MHz divided into 32 4 MHz channels. At 4.8 and 8.64 GHz, edge channels were removed and the central 24 channels averaged together to give a single channel for the analysis. At 1.34 GHz the central channels were maintained separately to remove phase smearing near the edges of the fields and to prevent possible Faraday depolarization across the band. The data reduction was done with the AIPS and MIRIAD packages. After editing and calibration were carried out, the mosaic images were formed using uniform weighting, and deconvolution was performed with CLEAN. The mosaicking operation automatically corrects for the primary beam response function. The total intensity image at 1.34 GHz was made with the multifrequency synthesis technique. In all cases the missing short spacings and the presence of bright nearby sources made confusion noise greater than the thermal system noise. This was particularly true for the total intensities, whereas the polarized intensities were weak enough that the theoretical noise levels were almost reached. The noise values listed in Table 1 were the measured values on the images.

For the polarization analysis, the images in the individual Stokes parameters Q and U were deconvolved separately

TABLE 2

FLUX DENSITIES OF G326.3−1.8

FREQUENCY (GHz)	FLUX DENSITY (mJy)		REFERENCE
	Entire SNR	Plerion	
0.408	180	...	Clark, Green, & Caswell 1975
0.843	153 ± 40	...	Milne et al. 1989
0.843	>130	22	Whiteoak & Green 1996
1.34	≫60	30	This paper
1.4	>95	...	Milne et al. 1979
2.65	115	...	Milne 1972
4.8	...	25	This paper
5.0	98	...	Milne 1969
5.0	75	...	Milne & Dickel 1975
8.4	68	...	Milne et al. 1989
8.64	...	15	This paper
8.8	...	<40	Dickel et al. 1973
14.7	69 ± 8	16 ± 7	Milne et al. 1979

and then combined to produce polarized intensity and position angle maps. The intensities were corrected for the Ricean bias that arises from the quadratic combination of two intensities. At 1.34 GHz, the initial data were combined into five 20 MHz channels to produce five polarized intensity and position angle maps. This sufficiently reduced the Faraday depolarization and also allowed good determination of the Faraday rotation between these channels across the full band so that no 180° ambiguities in position angle were present. The polarized intensity maps for the individual channels were subsequently averaged to produce a single map. At the higher frequencies, the Faraday depolarization effects are less significant, and the entire bandwidth was used for a single map at each frequency.

Flux density calibration was carried out using observations of PKS B1934−638. The antenna gains and polarization were calibrated by regular observations of PKS B1520−58 throughout the observing runs.

3. RESULTS

3.1. Total Intensity

3.1.1. Morphology

Figure 1 is a gray-scale image of the whole SNR at a frequency of 1.34 GHz with a half-power beamwidth of $8\rlap{.}''5 \times 6\rlap{.}''4$. The entire periphery of the remnant can be seen as a faint complete shell. This shell was not as obvious in previous lower resolution images (Milne et al. 1979; Whiteoak & Green 1996), which contained the full complement of short spacings between elements and showed the emission across the full face of the SNR. The overall emission appears to be more filled in toward the southwest of the plerion than it is around the rest of the remnant. The overall east-west alignment of filaments recognized in the previous images is also present in this ATCA image, primarily on the eastern side. Some of the individual filaments, particularly in the northwestern corner, appear unresolved but often sit on a smoother background that may contain several overlapping features. There are a number of faint optical filaments in G326.3−1.8, but they do not form a complete shell and several sit on the face of the remnant (van den Bergh 1979; Zealey et al. 1979; Dennefeld 1980; Rosado et al. 1996) where no particular radio enhancements are visible.

The new image also reveals structure within the plerion for the first time. This component of the SNR appears virtually identical at all three observing frequencies (see Fig. 2 for the 4.8 and 8.64 GHz images). It consists of several parallel ridges running along the major axis with some irregular patches at the ends. In particular, a circular ring is seen on the northwestern end. There is smooth emission between the ridges and over the interior of the ring. All of the individual features in the plerion appear to be resolved with half-power thicknesses of about 15″–20″.

3.1.2. Spectrum

As indicated above, it is impossible to measure the total flux density of the whole SNR even at 1.34 GHz because of the missing short spacings of the telescope array. The plerion, however, is smaller, and we have tried to estimate its integrated flux density at all three frequencies. The major difficulty remains the determination of the background level including emission from the shell component. By examination of various slices and images, we estimate the uncertainty to be about 33% of the values determined. These three values, together with all other published flux densities

for both the plerion and for the entire SNR, are listed in Table 2 and shown in Figure 3. Except for the few uncertainties listed, no other authors have been brave enough to give values for their uncertainties. We have assumed that they are all comparable and so have fitted the spectra with unweighted least-square lines.

The resultant spectra with power-law slopes of −0.29 for the whole SNR and −0.18 for the plerion are shown by the solid lines. The dashed line with a slope of −0.34 represents the spectrum of the whole SNR minus the plerion, or that of the shell component alone. Both components have spectral indices consistent with their classifications, although that of the shell is on the flat side of their distribution, similar to the well-known shell remnant IC 443 (Green 1998). The integrated flux density of the shell at 1 GHz is 114 Jy, which corresponds to a surface brightness of 1.23×10^{-20} W m^{-2} Hz^{-1} sr^{-1}. The plerion with a flux density of 26 Jy at 1 GHz has a surface brightness of 7.8×10^{-20} W m^{-2} Hz^{-1} sr^{-1}. Both values are about average for objects of their classification and size.

3.2. Polarization

The intensity of the shell at 1.34 GHz is too low to evaluate the polarization in detail, but in Figure 4, we show a gray-scale image of the polarized intensity with superimposed total-intensity contours. The plerion is bright and has a mean fractional polarization of 12%. Much of the apparent ring around the plerion in both total and polarized intensities is a grating response, but the polarized emission is stronger on the shell and does fill in somewhat southwest of the plerion toward the shell, just as the total intensity does. The subsequent discussion will concentrate on the plerion, which is significantly polarized at all three wavelengths. Because the resolution was about a factor of 2 better at the two higher frequencies, we will concentrate on those results.

Figure 5 shows the electric vectors of the polarized intensity at 4.8 GHz with superimposed total-intensity contours. For visibility on this and all other polarimetric maps, the vectors are spaced by 12″, or over 3 half-power beamwidths. This spacing also means that each vector is entirely independent. It can be seen that the polarized intensity follows the total intensity quite closely, and Figure 6 is a gray-scale image of the fractional polarization at 4.8 GHz with the same superimposed total-intensity contours. The mean fractional polarization is 35%, with no significant variation across the plerion. The results at 8.4 GHz are very similar, with a mean fractional polarization of 40%. These fractional values are very high for SNRs; they are likely artificially increased in the aperture synthesis observations because the polarized intensity probably has more fine structure than does the total intensity and the lack of short spacings between the antennas will misrepresent the background level under the plerion. Observations with the Parkes 63 m telescope find 20% at 8.4 GHz (Milne et al. 1989), 12% at 5 GHz (Milne & Dickel 1975; Whiteoak & Gardner 1971), and 2% at 2.7 GHz (Milne 1972) toward the peak of the plerion. Because the low resolution of the single-dish observations would smear the structure within the plerion, the true values probably lie between these extremes.

The position angles at 4.8 and 8.34 MHz can be used to evaluate the Faraday rotation. The results are shown in Figure 7, with filled squares indicating positive values of rotation measure and open squares negative values. The
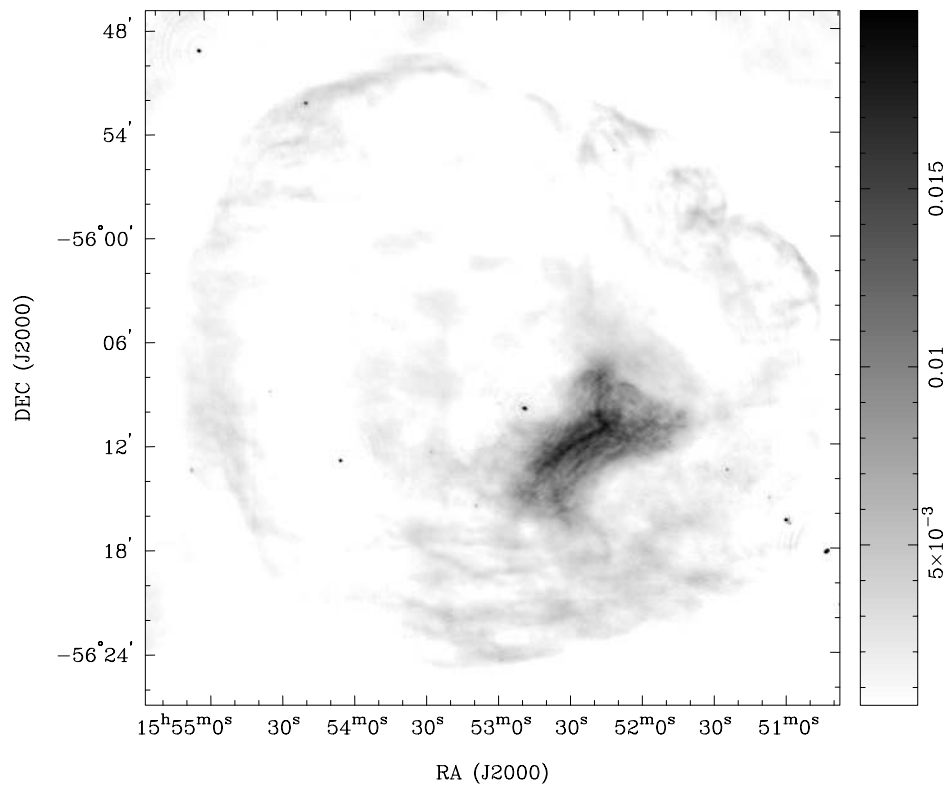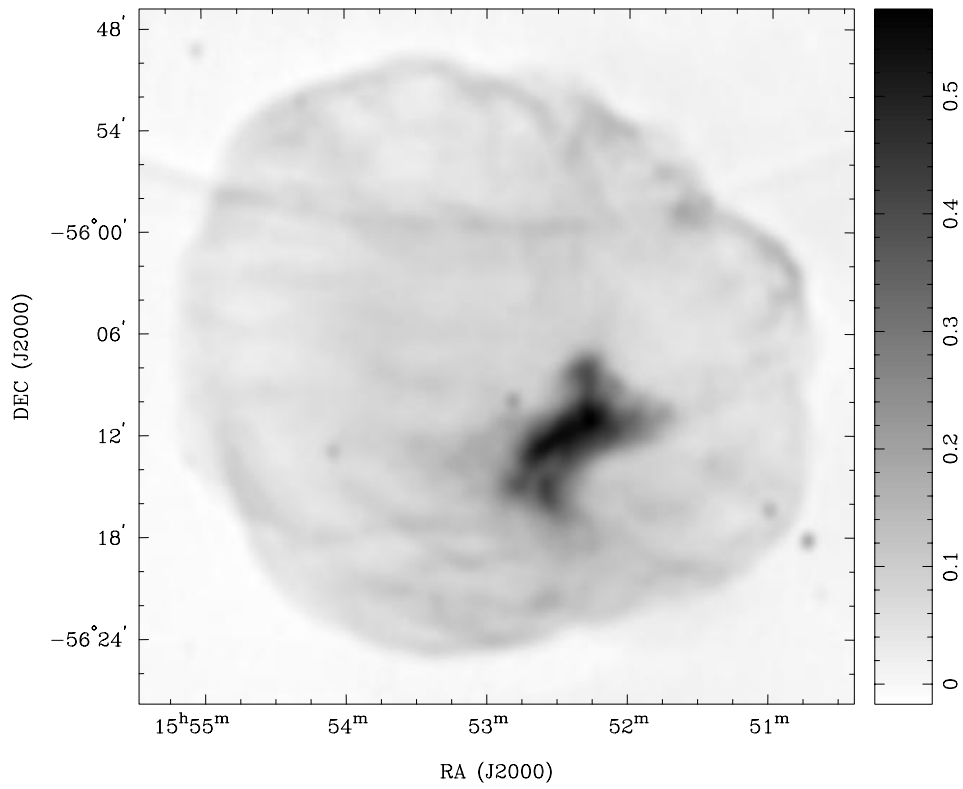
FIG. 1a

FIG. 1b

FIG. 1.—(a) Image of the composite supernova remnant G326.3 − 1.8 at a frequency of 1.34 GHz with a half-power beamwidth of 8″.5 × 6″.4. (b) Copy of the MOST image at 0.843 GHz with a resolution of 45″ for comparison.
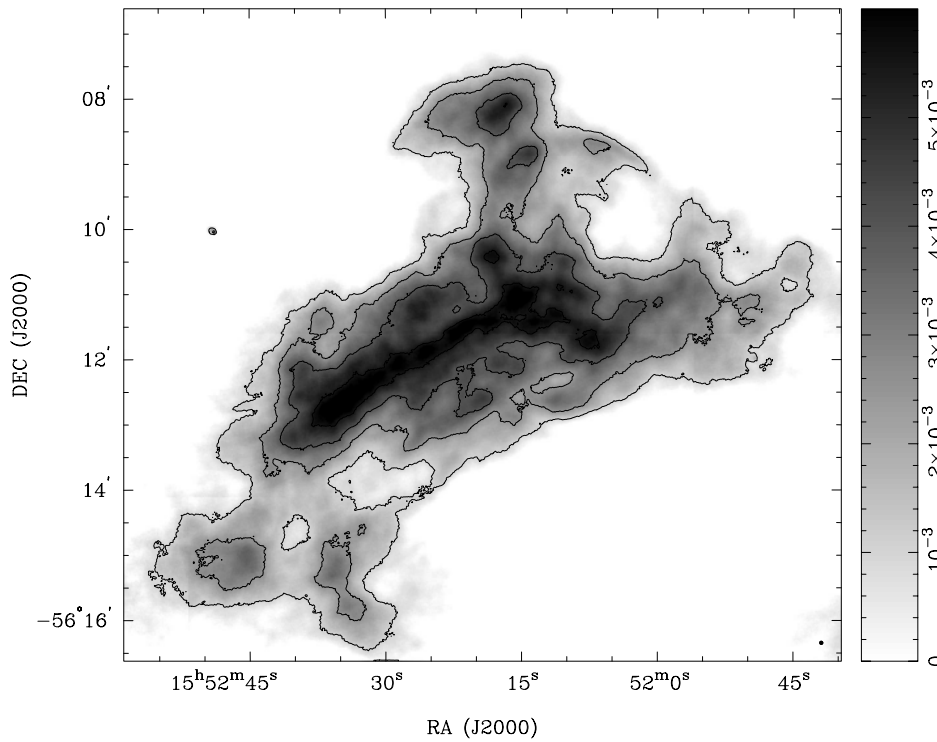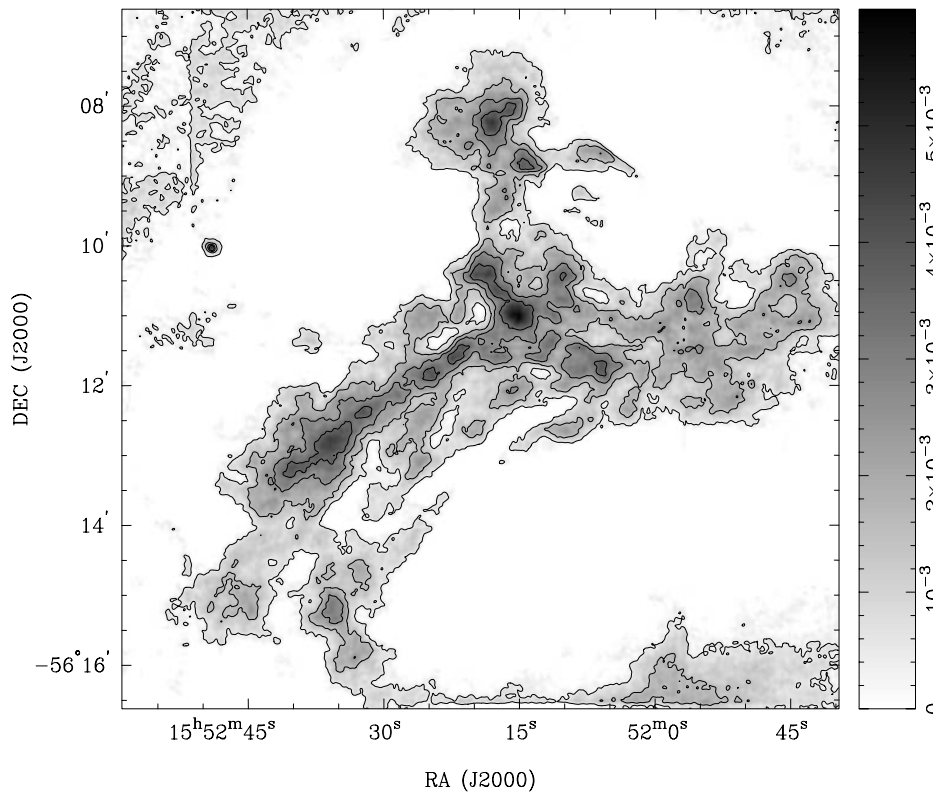
FIG. 2a

FIG. 2b

FIG. 2.—Images of the plerion component of the supernova remnant G326.3−1.8 at (a) 4.8 GHz with a circular half-power beamwidth of 3.8″ and (b) 8.64 GHz with a circular half-power beamwidth of 3.4″.

rotation measure is quite uniform at -300 rad m^{-2} with reliable values falling between -200 and -400 rad m^{-2}. The few positive values seen are probably not real, as they all lie near the edges of the image where the polarized inten-

sity is too weak to determine the rotation measure accurately.

Because the measured position angles can always have $180°$ ambiguities, there can be $n \times 180°$ additional
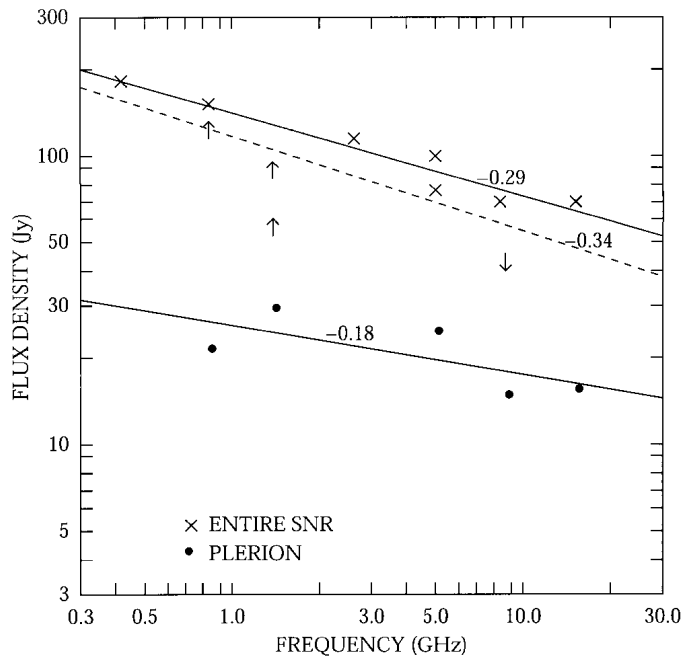
FIG. 3.—Radio spectrum of G326.3−1.8 from the data in Table 2. The crosses represent the entire SNR, and the dots represent only the plerion component. The upward and downward pointing arrows indicate upper and lower limits, respectively. The upper line is the fit for the whole SNR; the lower one is for the plerion; and the middle dashed line is the difference spectrum representing the shell part of this composite SNR.

rotation—either plus or minus—between the two frequencies. The 1.34 GHz results for the five adjacent 20 MHz bands, however, also give -300 rad m^{-2} for the rotation measure and thus confirm the adopted result.

The rotation measure can be used, in turn, to derotate the measured position angles to their zero-wavelength or intrinsic values. Figure 8 shows the actual direction of the *magnetic* field vectors of the plerion in G326.3−1.8. The lengths are proportional to the polarized intensity at 4.8 GHz, and the contours are, again, the total intensity at 4.8 GHz. We note that the field aligns beautifully with the ridges in the total intensity, and on the northwestern end of the plerion the field direction actually curves around to follow the ring structure.

4. DISCUSSION

G326.3−1.8 is a composite SNR with an evolutionarily old faint and thin shell but a bright plerion that may still be receiving input from an unseen pulsar. The shell looks like those that are well into the point-blast stage of development, in which the radius, R, expands as $R \propto t^{0.4}$, where t is time. The outline may be slightly flattened to the northwest but must be expanding fairly uniformly. The overall X-ray emission is fairly uniform with only marginal indications of a shell structure, but it does appear brighter toward the center and southeastern parts of the remnant (Kassim et al. 1993). Infrared data (Arendt 1989), on the other hand, show the apparent Galactic ridge to the northwest, so the
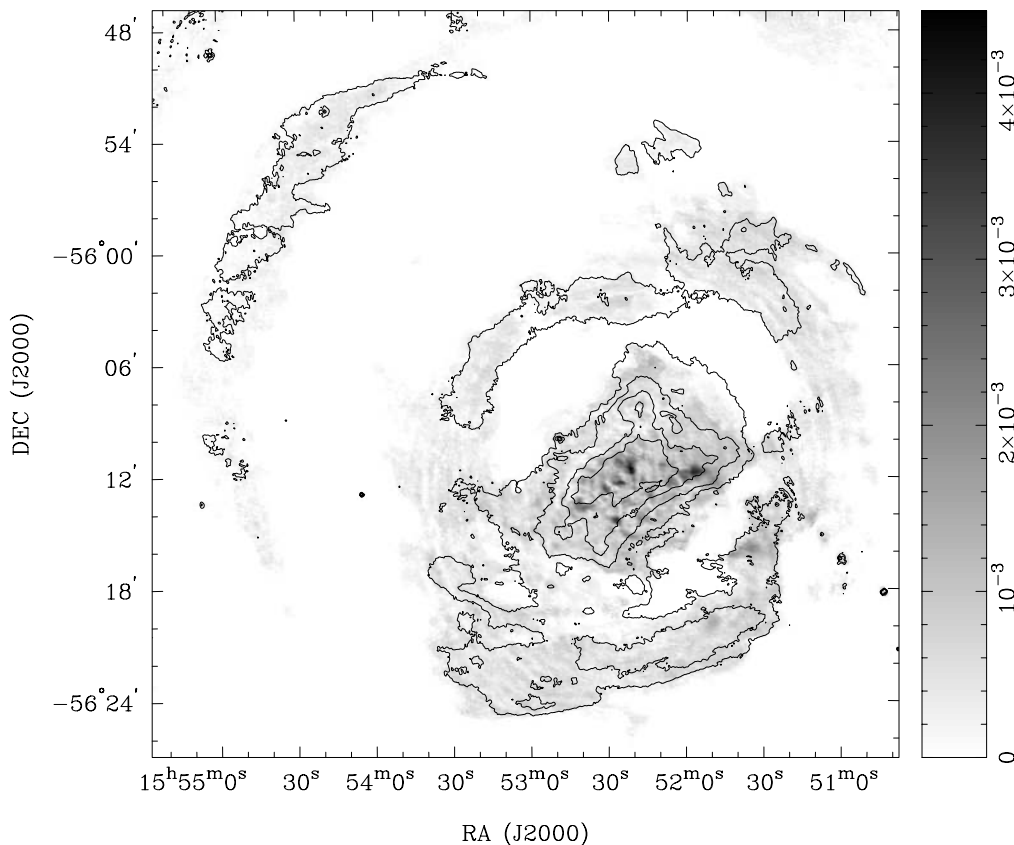

FIG. 4.—Gray scale of the polarized intensity of the supernova remnant G326.3−1.8 at a frequency of 1.34 GHz with selected superimposed contours of total intensity.
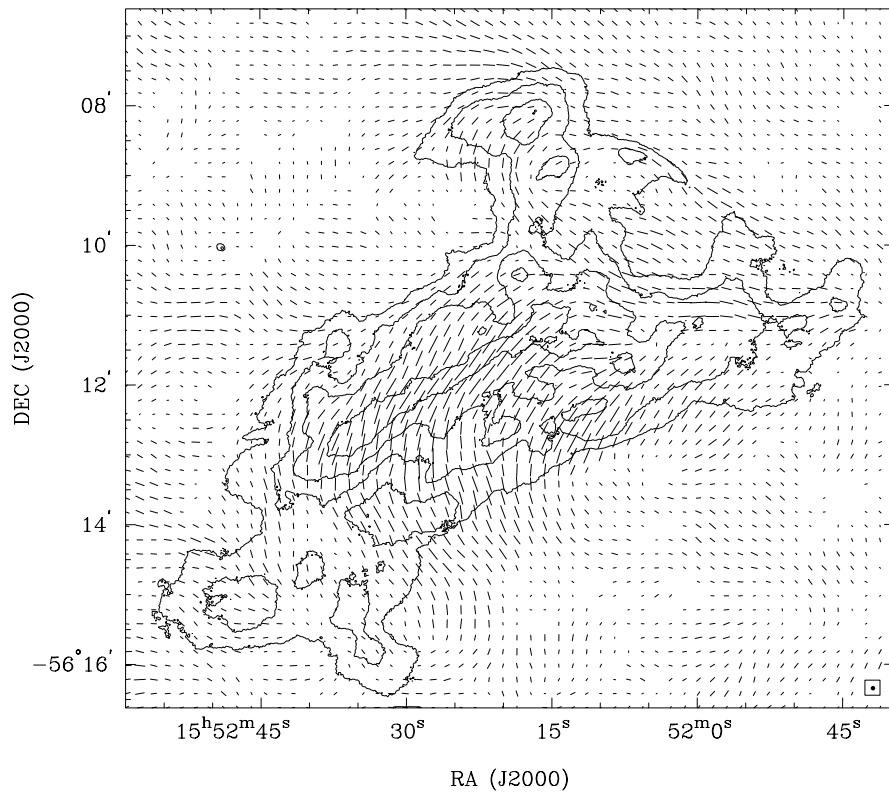
FIG. 5.—Electric vectors of the polarized emission from the plerion in the supernova remnant G326.3 − 1.8 at a frequency of 4.8 GHz with total intensity contours. A vector length of 4″ represents a brightness of 0.525 mJy beam^{-1}. The half-power beamwidth is shown by the dot within the box in the lower right corner of the map.
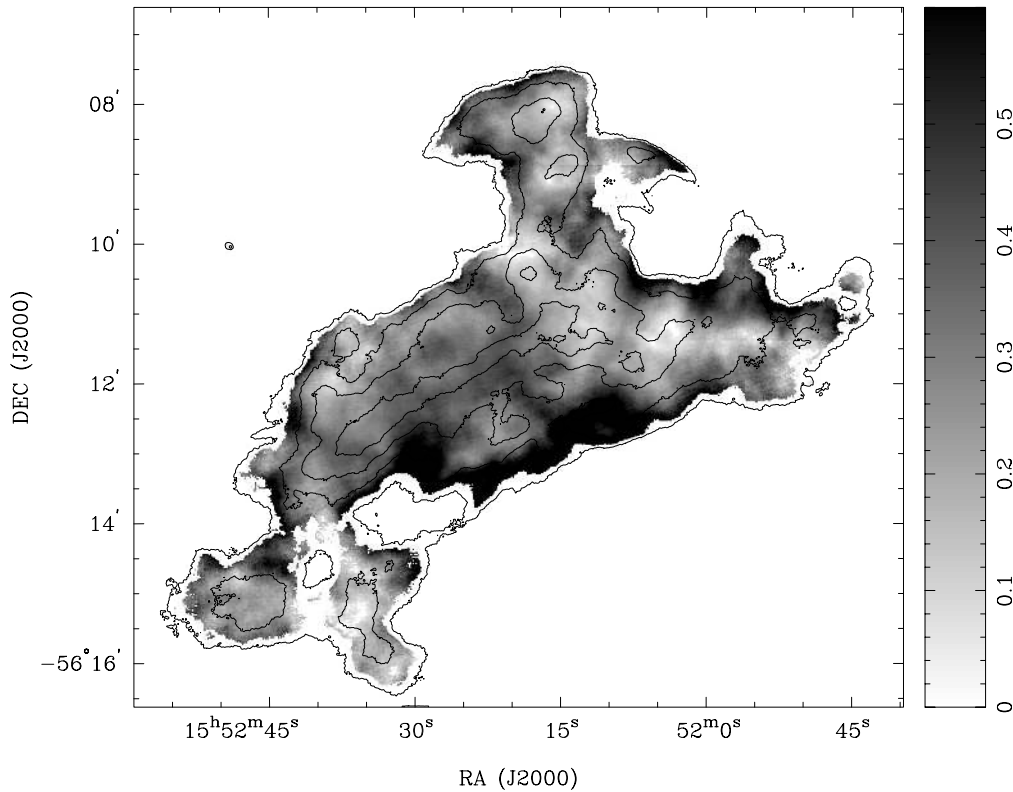

FIG. 6.—Gray scale of the fractional polarization of the plerion in the supernova remnant G326.3 − 1.8 at a frequency of 4.8 GHz with total intensity contours.
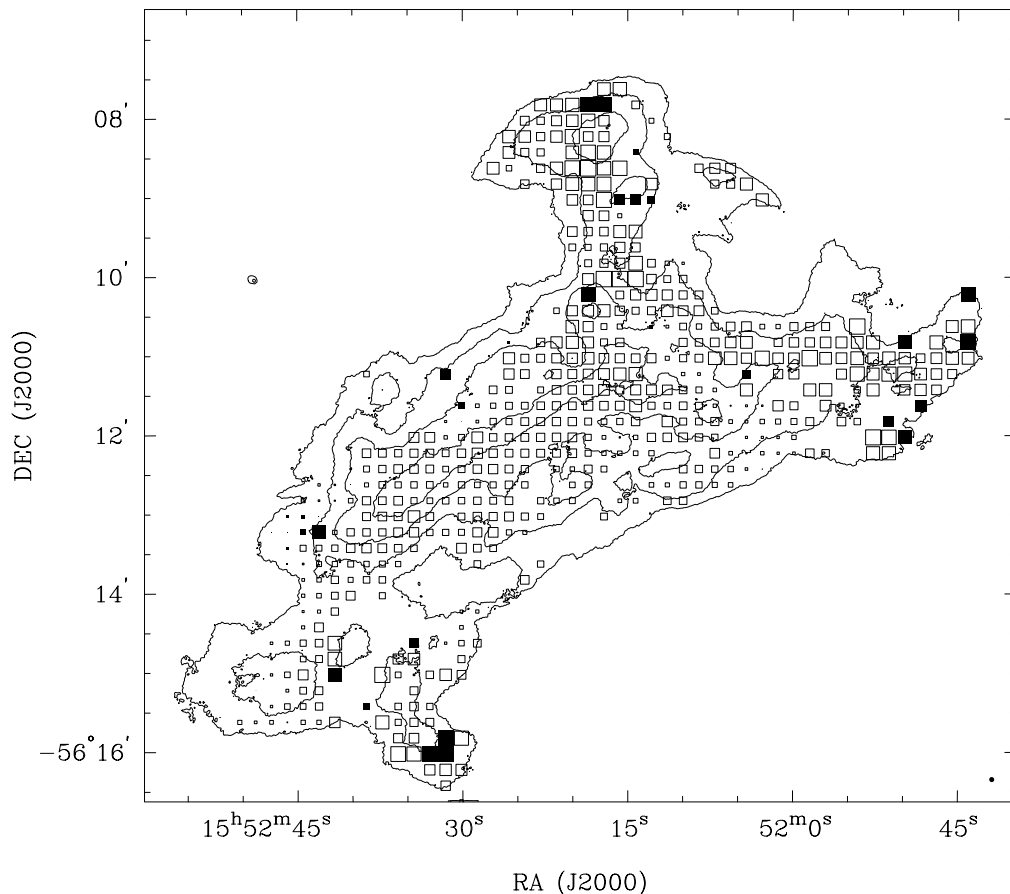
FIG. 7.—Faraday rotation measure toward the region of the plerion in the supernova remnant G326.3−1.8 with total intensity contours at a frequency of 4.8 GHz. Positive (*filled squares*) and negative (*open squares*) values of rotation measure are shown. A box dimension of 4″ represents a rotation measure of 200 rad m⁻².

reduction of apparent X-ray emission there could be absorption by intervening material that could also be beginning to interact with the expanding shell.

The lack of correlation of the radio and X-ray emission in the interior of this SNR is very unusual. The missing X-ray emission from the radio plerion is particularly hard to understand. It appears to be the only known plerion with strong radio emission but no X-rays. We note that, if anything, there is an indication of a decrease in the infrared structure at the position of the plerion (Arendt 1989). If radio emission trails behind a pulsar, the brightest part of the radio plerion could be behind the hardest X-rays. Such a situation appears to be true for the plerion N157B in the LMC (Lazendic et al. 2000), but there is still significant radio emission from the suspected position of the X-ray pulsar (Marshall et al. 1998; Wang & Gotthelf 1998) and significant X-ray emission from the position of the brightest radio emission in that object. A pulsar moving at perhaps 500 km s⁻¹ could have covered the approximately 8 pc distance from the center of the SNR to the radio plerion in about 15,000 yr and then have moved outward to the position of the current hard X-ray feature in about another 15,000 yr, leaving the plerion behind.

Estimation of the expected X-ray emission from the radio plerion requires knowledge of the spectrum of the emission between the X-ray and radio wavelengths. Theoretical predictions (Pacini & Salvati 1973; Reynolds & Chevalier 1984), with some observational support (Salter et al. 1989; Green & Scheuer 1992), indicate that the synchrotron emis-

sion generated by a pulsar should have a break in its spectrum from synchrotron radiation losses. This will move downward in frequency with time as the highest energy particles lose their energy the fastest. To determine the break frequency and thus the overall spectrum, we need to know the magnetic field strength. Using equations (5.7)–(5.12) of Ginzburg & Syrovatski (1965) for synchrotron emission, we find that the emission is proportional to the product of the relativistic electron energy and the magnetic field strength to the 1 α power, where α is the spectral index. Adopting the observed spectral index of −0.18 and the 1 GHz flux density of 26 Jy found above and then integrating the radio emission from 10 MHz to 100 GHz for the plerion at a distance of 4.1 kpc, we find an integrated luminosity of 3×10^{34} ergs s⁻¹. The total energy density in relativistic electrons radiating between 10 MHz and 100 GHz is then $9 \times 10^{42}/H^{1.18}$ ergs, where H is the magnetic field strength in gauss. The three-dimensional volume of the plerion is, of course, unknown, but we shall approximate it as a cylinder with a length of 12 pc and a radius of 3 pc. The energy density is then $1.8 \times 10^{-15}/H^{1.18}$ ergs cm⁻³. In Kepler's SNR (Matsui et al. 1984) and N23 in the LMC (Dickel & Milne 1998), the approximate ratio of relativistic electron energy to magnetic energy is about 3, so we will adopt this value to arrive at a mean magnetic field strength of 45 μG. This value is high for an old shell SNR but low for a young plerion where particle injection and magnetic field amplification are still occurring. It may indeed be appropriate for an older plerion. Such a field would give a break frequency
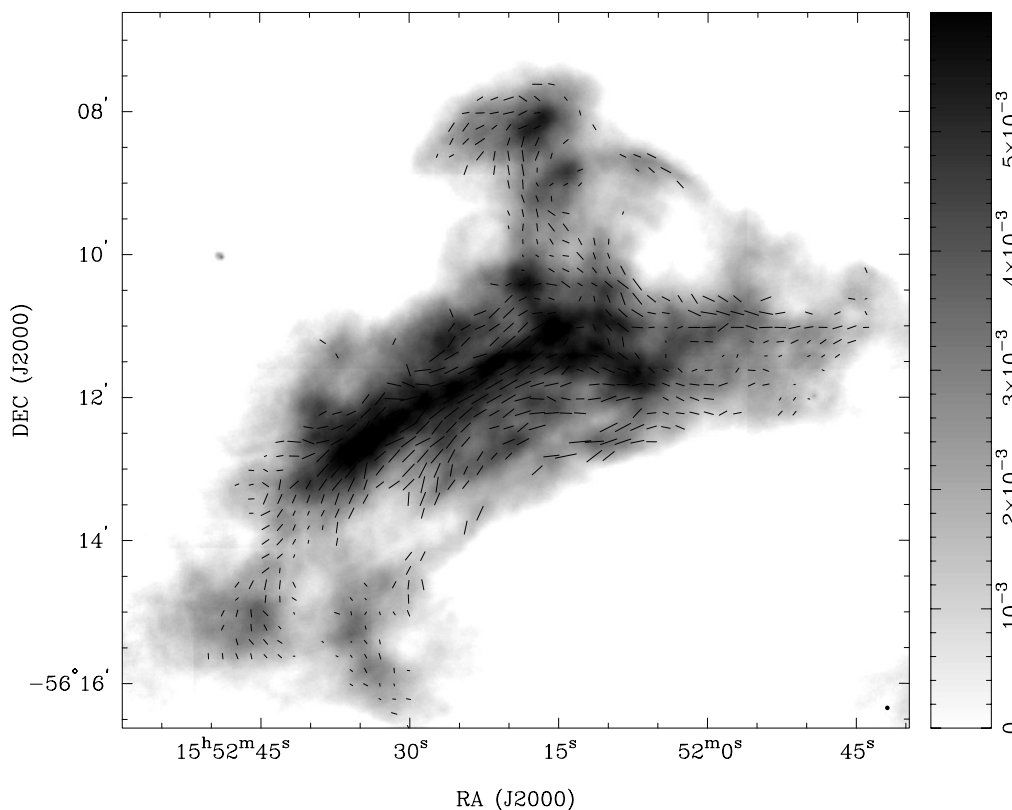
FIG. 8.—Vectors representing the direction of the magnetic field in the region of the plerion in the supernova remnant G326.3−1.8. The vector length represents the polarized intensity at 4.8 GHz, and the gray scale is the total intensity at 4.8 GHz.

near 1.6×10^{13} Hz for a lifetime of 3×10^4 yr. For this spectral break, the integrated 0.5–10 keV X-ray luminosity of the radio plerion should be about 2×10^{38} ergs s^{-1}, orders of magnitude above that detected toward the hard X-ray feature to the west. Even with large uncertainties in the parameter estimates, this must indeed be a very unusual source not to be detected in X-rays.

The extended feature in the *ASCA* hard X-ray band (2.5–9 keV) between the plerion and the shell to the southwest (Plucinsky 1998) is intriguing, as it might represent the current location of the pulsar presumed to be responsible for the various emission components. Although there is a slight increase in the overall radio emission in that general area, it appears as if it is a brightness enhancement on the face of the shell. There are also several optical filaments in that area (van den Bergh 1979; Dennefeld 1980), but there is no morphological association of any feature with the X-rays. The integrated X-ray emission is so faint, about 3×10^{33} ergs s^{-1} between 0.5 and 10 keV (Plucinsky 1998), however, that it would be missed by the radio surveys. Although we cannot measure the field in that direction, if the break frequency is the same as toward the radio plerion, the expected radio flux density at 1.34 GHz would be of order 0.5 mJy from the whole $6' \times 3'$ area of the hard X-ray source. Even with the 45″ beam of the MOST, such emission would not be detectable. We note that a stronger magnetic field, as might be expected near the pulsar, would move the break frequency lower and increase the expected radio emission, but the timescale near the pulsar is also shorter, which will work in the opposite direction to reduce the ratio of X-ray and radio emission.

One possible way to make G326.3−1.8 the necessary extreme case of particle injection and decay might be for it to have been a magnetar with an extremely high initial magnetic field so that it very quickly gave up most of its energy and stopped producing the hardest X-rays. The current production of X-ray– and radio-emitting particles is very low, but the lower energy electrons from the initial much more energetic pulsar would have persisted longer, and, as indicated above, they can still be radiating significantly after some thousands of years provided that the average magnetic field strength does not much exceed the current value of 45 μG estimated above.

The structure of the plerion is unusual, wherever the pulsar may be located. The morphology shows a bundle of parallel ridges running from southeast to northwest. Presumably injection from a pulsar could create one tube or perhaps a spiral pattern, e.g., SS 433 (Hjellming & Johnston 1981), but it is difficult to see how to get the aligned structures, much less the ring with a diameter of about 3.6 pc at one end. The motion of any pulsar relative to the observed structures also remains unclear. If it started in the center of the remnant and moved outward to the present position of the hard X-ray component, the nearly perpendicular plerion coming out from one side near the middle of the path is very peculiar. If the ring structure represents a bubble around the original position of the pulsar and the pulsar then moved along the axis of the plerion, it had to make an abrupt turn to get to the present location of the hard X-rays. Detection of a pulsar and measurements of its proper motion would greatly aid in understanding this peculiar object.

The magnetic field is also aligned along the ridges but wraps around with the ring structure on the northwestern end (Fig. 8). The relatively high fractional polarization and very uniform Faraday rotation suggest that there is little internal Faraday effect and that the magnetic field is quite uniform. The field is probably frozen into the fluid structure. Unfortunately, it is not possible to determine the thermal energy and pressure to see whether that dominates the magnetic field in the plerion since it is seen only in radio synchrotron emission.

5. SUMMARY

As often happens in astronomy, the first identified object in the class of composite SNRs is one of the most unusual. While the shell component appears quite normal, the plerion has several unique characteristics. It is certainly one of the largest and brightest plerions relative to its shell, although there are several apparently naked plerions that are larger, including G328.4+0.2 (Gaensler, Dickel, & Green 2000), N157B (Chu et al. 1992; Lazendic et al. 2000) with a detected 16 ms X-ray pulsar (Marshall et al. 1998), and G74.9+1.2 (Weiler & Shaver 1978), all of which reach a diameter of about 25 pc.

While most plerions are elongated like that in G326.3−1.8, they generally show a rather amorphous or irregular structure rather than the apparent bundle of parallel filaments seen in this object. Furthermore, the ring on the northwestern end might be a preexisting bubble or somehow related to the pulsar and plerion. The magnetic field strength is moderate, and the field follows the direction of the ridges but also circles around the ring.

There is no X-ray emission specifically associated with the very bright radio plerion. Perhaps if the stellar remains of the supernova explosion had been a magnetar with a magnetic field strength of $\sim 10^{15}$ G and rapid energy loss, the initial emission would have been very bright but have dropped quickly. The break frequency in the synchrotron spectrum could also have dropped quickly but then would have slowed as the plerion expanded and the magnetic field strength dropped. This process could reduce the X-ray emission quickly but leave significant radio emission. The very faint hard X-ray emission to the southwest of the radio plerion could represent what is left of the stimulation by the magnetar.

REFERENCES

Arendt, R. G. 1989, ApJS, 70, 181
Caswell, J. L., Murray, J. D., Roger, R. S., Cole, D. J., & Cooke, D. J. 1975, A&A, 45, 239
Chu, Y.−H., Kennicutt, R. C., Jr., Schommer, R. A., & Laff, J. 1992, AJ, 103, 1545
Clark, D. H., Green, A. J., & Caswell, J. L. 1975, Australian J. Phys. Astrophys. Suppl., 37, 75
Dennefeld, M. 1980, PASP, 92, 603
Dickel, J. R., & Milne, D. K. 1998, AJ, 115, 1057
Dickel, J. R., Milne, D. K., Kerr, A. R., & Ables, J. G. 1973, Australian J. Phys., 26, 379
Frail, D., Giacani, E. B., Goss, W. M., & Dubner, G. M. 1996, ApJ, 464, L165
Frater, R. H., Brooks, J. W., & Whiteoak, J. B. 1992, J. Electr. Electron. Eng. Australia, 12, 103
Gaensler, B. M., Dickel, J. R., & Green, A. J. 2000, ApJ, 542, 380
Giacani, E. B., Kassim, N. E., Frail, D. A., Goss, W. M., Winkler, P. F., & Williams, B. F. 1997, AJ, 113, 1379
Ginzburg, V. L., & Syrovatski, S. I. 1965, ARA&A, 3, 297
Green, D. A. 1998, http://www.mrao.cam.ac.uk/surveys/snrs/
Green, D. A., & Scheuer, P. A. G. 1992, MNRAS, 258, 833
Hjellming, R. M., & Johnston, K. J. 1981, ApJ, 246, L141
Kassim, N., Hertz, P., & Weiler, K. W. 1993, ApJ, 419, 733
Kesteven, M. J., & Caswell, J. L. 1987, A&A, 183, 118
Lazendic, J. S., Dickel, J. R., Haynes, R. F., Jones, P. A., & White, G. L. 2000, ApJ, 540, 808
Manchester, R. N., Staveley-Smith, L., & Kesteven, M. J. 1993, ApJ, 411, 756

Marshall, F. E., Zhang, W., Gotthelf, E. V., Middleditch, J., & Wang, Q. D. 1998, ApJ, 499, L179
Matsui, Y., Long, K. S., Dickel, J. R., & Greisen, E. W. 1984, ApJ, 287, 295
Mills, B. Y., Slee, O. B., & Hill, E. R. 1961, Australian J. Phys., 14, 497
Milne, D. K. 1969, Australian J. Phys., 22, 613
─────. 1972, Australian J. Phys., 25, 307
Milne, D. K., Caswell, J. L., Kesteven, M. J., Haynes, R. F., & Roger, R. S. 1989, Publ. Astron. Soc. Australia, 8, 187
Milne, D. K., & Dickel, J. R. 1975, Australian J. Phys., 28, 209
Milne, D. K., Goss, W. M., Haynes, R. F., Wellington, K. J., Caswell, J. L., & Skellern, D. J. 1979, MNRAS, 188, 437
Pacini, F., & Salvati, M. 1973, ApJ, 186, 249
Plucinsky, P. 1998, Mem. Soc. Astron. Italiana, 69, 939
Reynolds, S. P., & Chevalier, R. A. 1984, ApJ, 278, 630
Rosado, M., Ambrocio-Cruz, P., LeCoarer, E., & Marcelin, M. 1996, A&A, 315, 243
Salter, C., Reynolds, S., Hogg, D., Payne, J., & Rhodes, P. 1989, ApJ, 338, 171
Seward, F. D., Harnden, F. R., & Helfand, D. J. 1984, ApJ, 287, L19
van den Bergh, S. 1979, ApJ, 227, 497
Wang, Q. D., & Gotthelf, E. V. 1998, ApJ, 509, L109
Weiler, K. W., & Shaver, P. A. 1978, A&A, 70, 389
Weiler, K. W., & Sramek, R. 1988, ARA&A, 26, 295
Whiteoak, J. B., & Gardner, F. F. 1971, Australian J. Phys., 24, 913
Whiteoak, J. B. Z., & Green, A. J. 1996, A&AS, 118, 329
Zealey, W. J., Elliott, K. H., & Malin, D. F. 1979, A&AS, 38, 39